Eur. Phys. J. A **18**, 597–604 (2003)
DOI 10.1140/epja/i2003-10099-9

THE EUROPEAN PHYSICAL JOURNAL A

A model for A = 3 antinuclei production in proton-nucleus collisions

R.P. Duperray[a], K.V. Protasov[b], L. Derome[c], and M. Buénerd[d]

Laboratoire de Physique Subatomique et de Cosmologie, IN2P3-CNRS, UJFG, 53, Avenue des Martyrs, F-38026 Grenoble Cedex, France

Received: 28 January 2003 / Revised version: 10 July 2003 /
Published online: 18 November 2003 –
Communicated by A. Molinari

Abstract. A simple coalescence model based on the same diagrammatic approach of antimatter production in hadronic collisions as used previously for antideuterons is used here for the hadroproduction of mass-3 antinuclei. It is shown that the model is able to reproduce the existing experimental data on the $\overline{t}$ and $\overline{^3\mathrm{He}}$ production without any additional parameter.

PACS. 24.10.-i Nuclear reaction models and methods

1 Introduction

The increasing interest in the study of production of light antinuclei in proton-proton and proton-nucleus collisions is motivated by the presence of antinuclei in cosmic rays which has potentially important implications on the matter-antimatter asymmetry of the Universe. From this point of view, it is important to determine the amount of antimatter which can be produced in the galaxy through the interaction of high-energy protons with the interstellar gas. A new generation of experiments (AMS [1], PAMELA [2]) should be able to measure the flux of antimatter in a near future.

The calculations of the $\overline{t}$ and $\overline{^3\mathrm{He}}$ production cross-sections reported here are based on the same diagrammatic approach to the coalescence model as used recently [3] to describe the $\overline{d}$ production in proton-proton and proton-nucleus collisions.

The usual coalescence model [4] is based on the simple hypothesis that the nucleons, produced during the collision of a beam and a target, fuse into light nuclei whenever the momentum of their relative motion is smaller than a coalescence radius p_0 in the momentum space, which is a free parameter of the model, usually fit to the experimental data (see [5] for example). A simple diagrammatic approach to the coalescence model developed in [6] provided a microscopic basis to the model. In this approach, the parameter p_0 is expressed in terms of the slope parameter of the inclusive nucleon production spectrum and of the wave function of the produced nucleus.

This diagrammatic approach has been generalized in [3] to antideuteron production by taking into account threshold effects and the anisotropy of the angular distributions. This approach can reproduce most existing data without any additional parameter in energy domains where the inclusive antiproton production cross-sections are well known.

This article reports on the application of this approach to the production of $A = 3$ antinuclei. It is the first microscopic calculation of this cross-section to the knowledge of the authors. In [7], the $\overline{^3\mathrm{He}}$ production cross-section in proton-proton collisions was calculated using the standard coalescence model, with the parameter p_0 taken from the $\overline{d}$ production data.

Unfortunately, the experimental data required to be compared with the calculations are limited. Only two sets of experiments have measured the production of mass-3 antinuclei in proton-nucleus collisions. $\overline{t}$ and $\overline{^3\mathrm{He}}$ were discovered at IHEP (Serpukhov), with one experimental point measured for $\overline{t}$ and one for $\overline{^3\mathrm{He}}$ [8,9], while in the CERN experiment (SPS, WA 33) [10,11], four experimental points were measured for $\overline{t}$ and eight for $\overline{^3\mathrm{He}}$. For these latter data however, the $\overline{t}$ and $\overline{^3\mathrm{He}}$ production cross-sections were measured with respect to the pion production cross-section at the same momentum. This requires the corresponding experimental values of the pion production cross-section to be known to extract the values of the $\overline{t}$ and $\overline{^3\mathrm{He}}$ production cross-sections.

The article is organized as follows. The main ideas of the theoretical approach are described in sect. 2. The

[a] e-mail: duperray@lpsc.in2p3.fr
[b] e-mail: protasov@lpsc.in2p3.fr
[c] e-mail: derome@lpsc.in2p3.fr
[d] e-mail: buenerd@lpsc.in2p3.fr

formalism is generalized to the case of $A = 3$ antinuclei production in sect. 3. Section 4 is devoted to the results and the comparison to the experimental data. A brief summary of the work is provided before the work is concluded in the last section.

2 Diagrammatic approach to the coalescence model

The main ideas of the diagrammatic approach of the coalescence model for nuclear fragment production are reminded here for the reader's convenience [6]. The simplest Feynman diagram of fig. 1 corresponding to fusion of three nucleons is considered as a basis for the coalescence model. Here the symbol f designates the state of all particles but nucleons 1, 2 and 3 which form the tritium or the helium-3 nucleus produced in the final state (specified by the t-symbol in the graph).

The physical picture behind this diagram is quite simple: the nucleons produced in a collision (block A) are "slightly" virtual and can fuse without any further interaction with the nuclear field. This diagram is not the only possible contribution to the full transition amplitude. However, as was shown in [12], where various diagrams were considered, there are mutual cancellations of a number of diagrams. As a result, at sufficiently large deuteron momenta the diagram of fig. 1 is the dominant one, and at this stage the other diagrams can be neglected.

This diagram can be calculated using the technique developed in [13]. The probability for three-nucleon coalescence is given by

$$\mathrm{d}^3W_t = |M|^2 \frac{m_t}{E_t} \frac{\mathrm{d}^3p_t}{(2\pi)^3}\,, \tag{1}$$

where m_t in the mass of the t fragment and E_t its energy in the (beam)nucleon-(target)nucleon center-of-mass system of the colliding nuclei. The probability for three-nucleon production is then

$$\mathrm{d}^9W_{123} = |M_{\mathrm{A}}|^2 \frac{m_p}{E_1} \frac{\mathrm{d}^3p_1}{(2\pi)^3} \frac{m_p}{E_2} \frac{\mathrm{d}^3p_2}{(2\pi)^3} \frac{m_p}{E_3} \frac{\mathrm{d}^3p_3}{(2\pi)^3}\,, \tag{2}$$

where M_{A} is the amplitude corresponding to the block A, *i.e.*, accounting for the inclusive production of nucleons 1, 2 and 3 and other particles in the final state f. To avoid cumbersome expressions in eqs. (1) and (2), the factors corresponding to colliding nuclei have been omitted since they cancel in further calculations. Using the conventional graph technique [13], the expression for M can be written in the form

$$\begin{aligned} M = & \int \frac{\mathrm{d}^4p_1}{(2\pi)^4} \int \frac{\mathrm{d}^4p_2}{(2\pi)^4} \int \frac{\mathrm{d}^4p_3}{(2\pi)^4} \\ & \times \frac{2m_p}{m_p^2 - p_1^2 - i0} \frac{2m_p}{m_p^2 - p_2^2 - i0} \frac{2m_p}{m_p^2 - p_3^2 - i0} \\ & \times i\,(2\pi)^4\,\delta^4\,(p_1 + p_2 + p_3 - p_t) \\ & \times M_{(1,2,3\to t)} M_{\mathrm{A}}\,, \end{aligned} \tag{3}$$

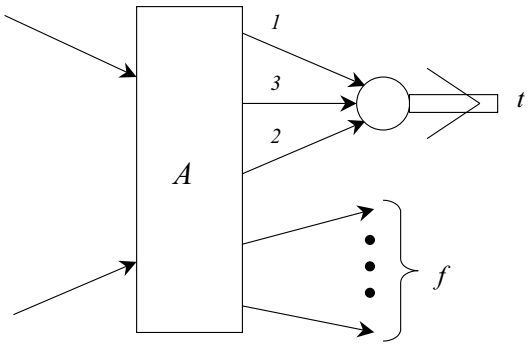

Fig. 1. The simplest Feynman diagram corresponding to coalescence of three nucleons into a tritium or ^{3}He.

where $M_{(1,2,3\to t)}$ is the vertex of coalescence of 1, 2, 3 into t (proportional to the three-nucleon wave function in the momentum space in the nonrelativistic approximation), m_p the nucleon mass, the three fractions being the individual nucleon propagators of 1, 2 and 3. The integrals have to be performed over energies and momenta of the (virtual) particles. The delta-functions ensure energy momentum conservation at the t vertex, $p_t = (\mathbf{p}_t, E_t)$, with $\mathbf{p}_t = \mathbf{p}_1 + \mathbf{p}_2 + \mathbf{p}_3$ being the momentum of t, E_t its energy. The dependence of the amplitude M_{A} on its variables (the particle momenta) is also needed explicitly for the calculations. In lack of a reliable theoretical form, this can be done in a "minimal" way, by using empirical shapes. The inclusive nucleon spectra usually have a decreasing form which can be approximated by a Gaussian function in the center-of-mass frame:

$$E_p \frac{\mathrm{d}^3\sigma_p}{\mathrm{d}p_p^3} \propto \exp\left(-\mathbf{p}_p^2/Q^2\right)\,, \tag{4}$$

where Q defines the slope parameter of the momentum distribution. Accordingly, the amplitude M_{A} can be written in the following way:

$$\begin{aligned} M_{\mathrm{A}} &= C \exp\left(-\frac{\mathbf{p}_1^2 + \mathbf{p}_2^2 + \mathbf{p}_3^2}{2Q^2}\right) \\ &= C \exp\left(-\frac{\mathbf{p}_t^2}{6Q^2}\right) \exp\left(-\frac{\mathbf{q}^2}{Q^2}\right) \exp\left(-\frac{3\mathbf{p}^2}{4Q^2}\right)\,, \end{aligned} \tag{5}$$

where

$$\begin{aligned} \mathbf{p}_t &= \mathbf{p}_1 + \mathbf{p}_2 + \mathbf{p}_3, \\ \mathbf{p} &= \frac{1}{\sqrt{3}}\,(\mathbf{p}_1 - \mathbf{p}_2)\,, \\ \mathbf{q} &= \frac{1}{2\sqrt{3}}\,(\mathbf{p}_1 + \mathbf{p}_2 - 2\mathbf{p}_3)\,. \end{aligned} \tag{6}$$

Assuming a statistical independence in the three-nucleon production process, the inclusive production cross-section can be written as the product of the three independent probabilities:

$$\frac{\mathrm{d}^9W_{123}}{\mathrm{d}p_1^3\mathrm{d}p_2^3\mathrm{d}p_3^3} = \frac{1}{\sigma_{\mathrm{inel}}^2} \frac{\mathrm{d}^3W_1}{\mathrm{d}p_1^3} \frac{\mathrm{d}^3W_2}{\mathrm{d}p_2^3} \frac{\mathrm{d}^3W_3}{\mathrm{d}p_3^3}\,, \tag{7}$$

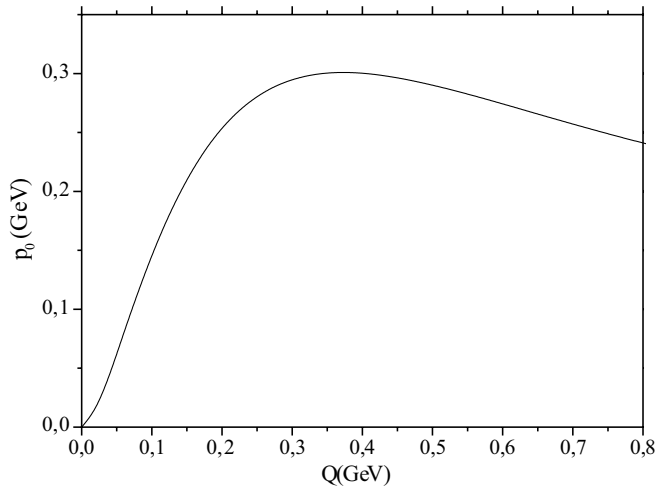

Fig. 2. Dependence of the coalescence momentum p_0 on the slope parameter Q of the inclusive nucleon spectrum.

where $\sigma_{\rm inel}$ is the total reaction cross-section of the colliding particles.

After integration of (3), taking into account (5) and (7), and dividing by the incident particle flux, the t production cross-section takes the form

$$E_t \frac{\mathrm{d}^3\sigma_t}{\mathrm{d}p_t^3} = \frac{96\pi^6}{m_p^2\sigma_{\rm inel}^2} |S|^2 E_1 \frac{\mathrm{d}^3\sigma_1}{\mathrm{d}p_1^3} E_2 \frac{\mathrm{d}^3\sigma_2}{\mathrm{d}p_2^3} E_3 \frac{\mathrm{d}^3\sigma_3}{\mathrm{d}p_3^3} , \quad (8)$$

with $\mathbf{p}_1 = \mathbf{p}_2 = \mathbf{p}_3$, $\mathbf{p}_t = 3\mathbf{p}_1$ and

$$S = \int \exp\left(-\frac{\mathbf{q}^2}{Q^2} - \frac{3}{4}\frac{\mathbf{p}^2}{Q^2}\right) \Psi_t(\mathbf{p},\mathbf{q}) \frac{\mathrm{d}^3\mathbf{p}}{(2\pi)^3} \frac{\mathrm{d}^3\mathbf{q}}{(2\pi)^3} , \quad (9)$$

where $\Psi_t(\mathbf{p},\mathbf{q}) \propto M_{123\to t}$ is the wave function of the t (or ^{3}He) system normalized by the condition

$$\int |\Psi_t(\mathbf{p},\mathbf{q})|^2 \frac{\mathrm{d}^3\mathbf{p}}{(2\pi)^3} \frac{\mathrm{d}^3\mathbf{q}}{(2\pi)^3} = 1 . \quad (10)$$

The factor 1/2, which accounts for nucleons and $A = 3$ nuclei spins, is included in (8). The three-nucleon wave function is needed at sufficiently large momenta to compute the amplitude. The wave function of [14] has been used (see appendix A for discussion).

The structure of (8) is the same as that of the coalescence model and the S integral in (8) can be straightforwardly related to the coalescence momentum:

$$p_0^3 = 18\sqrt{3}\pi^2 \int \frac{\mathrm{d}^3\mathbf{p}}{(2\pi)^3} \frac{\mathrm{d}^3\mathbf{q}}{(2\pi)^3} \times \exp\left(-\frac{\mathbf{q}^2}{Q^2} - \frac{3}{4}\frac{\mathbf{p}^2}{Q^2}\right) \Psi_t(\mathbf{p},\mathbf{q}) . \quad (11)$$

As an example, in fig. 2, the values of p_0 as a function of Q (eq. (11)) are presented for the wave function of [14]. Thus, in the approach based on the diagram of fig. 1 and within the approximations made above, the coalescence momentum p_0 is not an adjustable parameter anymore, but it is determined by the inclusive proton spectrum and by the trinucleon wave function. Note that in that case, p_0 depends on the momentum distribution and should thus be energy and system dependent.

3 Application to three-antinuclei production

In order to generalize the diagrammatic approach of the coalescence model to the production of $A = 3$ antinuclei (noted as $\overline{t}$ further below), two effects have to be taken into account: the anisotropy of angular distributions and the threshold effects [3]. Isotropic angular dependence is frequently assumed in nonrelativistic collisions. However, in relativistic collisions, the momentum distributions are strongly anisotropic and the low-energy approximation cannot be used. To take this into account, formula (8) can be easily generalized to any angular dependence. Assuming the inclusive nucleon production cross-section to be given by the (parameterized) amplitude $M_1(\mathbf{p}_1)$,

$$E_1 \frac{\mathrm{d}^3\sigma_1}{\mathrm{d}p_1^3} = |M_1(\mathbf{p}_1)|^2 , \quad (12)$$

In the general case, however, the inclusive (anti)nucleon production is not a Gaussian as in relation (4), which depends only on $\mathbf{p}_p^2$, but a functional form which depends on the inclusive kinematic variables (see appendix B). The cross-section for the t production can then be written (see (8)) as

$$E_t \frac{\mathrm{d}^3\sigma_t}{\mathrm{d}p_t^3} = \frac{96\pi^6}{m_p^2\sigma_{\rm inel}^2} \left[\int M_1(\mathbf{p}_1) M_2(\mathbf{p}_2) M_3(\mathbf{p}_3) \times \Psi_t(\mathbf{p},\mathbf{q}) \frac{\mathrm{d}^3\mathbf{p}}{(2\pi)^3} \frac{\mathrm{d}^3\mathbf{q}}{(2\pi)^3} \right]^2 . \quad (13)$$

Note that, in (13), the coalescence momentum p_0 does not appear directly, in this model; it can be ignored although it is a useful phenomenological parameter. This model could be practically used directly to describe the production of $\overline{t}$. The production threshold of the antiparticle has to be taken into account, however, in the cross-section calculation. The same procedure to evaluate the cross-section near threshold as that used in [3], will be applied here. In nucleon-nucleon collisions, the main reaction producing a $\overline{t}$ particle is $NN \to \overline{t} + 5N$. Near the threshold of this reaction, the energy dependence of the $\overline{t}$ production cross-section is mostly governed by the five-nucleons phase space $\Phi\left(\sqrt{s + m_{\overline{t}}^2 - 2\sqrt{s}E_{\overline{t}}}; 5m_p\right)$:

$$E_{\overline{t}} \frac{\mathrm{d}^3\sigma_{\overline{t}}}{\mathrm{d}p_{\overline{t}}^3} \propto \Phi\left(\sqrt{s + m_{\overline{t}}^2 - 2\sqrt{s}E_{\overline{t}}}; 5m_p\right) . \quad (14)$$

The phase space Φ for n particles with masses, momenta and energies, m_i, $\mathbf{p}_i$, and E_i, respectively, is defined in the usual way (in the center of mass):

$$\Phi(\sqrt{s}; m_1, m_2, \ldots m_n) = \prod_{i=1}^{n} \frac{1}{(2\pi)^3} \frac{\mathrm{d}^3 p_i}{2E_i} \delta^3\left(\sum_{i=1}^{n} \mathbf{p}_i\right) \delta\left(\sum_{i=1}^{n} \mathbf{E}_i - \sqrt{s}\right) .$$

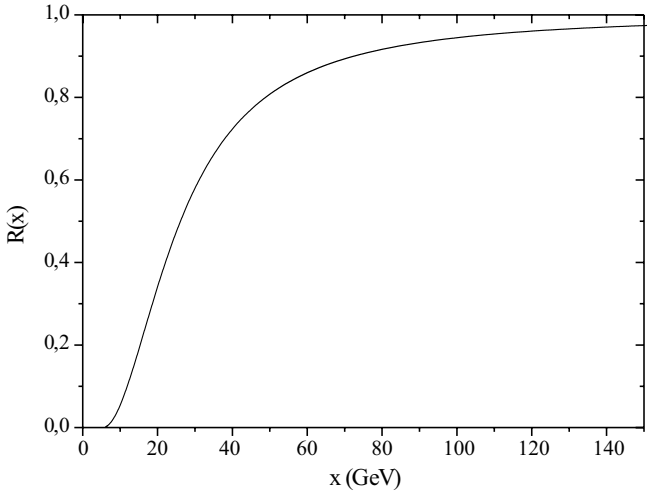

Fig. 3. Dependence of the threshold factor $R(x)$, with x as defined in the text.

It was calculated here by using the standard CERN library program (W515, subroutine GENBOD) [15]. $\sqrt{s}$ is the total energy of the n particles in the center-of-mass system.

A phenomenological correction factor R can thus be introduced in formula (13) which then reads

$$R\left(x\right) = \frac{\Phi\left(x; 5m_p\right)}{\Phi\left(x; 5 \times 0\right)}\,, \tag{15}$$

where $x = \sqrt{s + m_t^2 - 2\sqrt{s}E_{\overline{t}}}$, and where the denominator contains the high-energy limit of the phase space to ensure R to be dimensionless and not to change the value of the cross-section out of the space phase boundary. The limits of R are thus

$$R \to 0, \qquad E_{\overline{t}} \to E_{\overline{t}}^{\max} = \frac{s + m_t^2 - \left(5m_p\right)^2}{2\sqrt{s}}\,,$$

$$R \to 1, \qquad \sqrt{s} \to \infty\,.$$

If $p_{\overline{t}}^2 \ll (\sqrt{s} - E_{\overline{t}})^2$, the expression $\sqrt{s + m_t^2 - 2\sqrt{s}E_{\overline{t}}}$ can be replaced by $\sqrt{s} - E_{\overline{t}}$. This same approximation was made in [3]. The functional dependence of $R(x)$ is shown in fig. 3.

4 Results on antinuclei production data

4.1 Status of the data

This section is introduced with a brief overview of the current experimental situation on the antinuclei production relevant to the present study, *i.e.*, in proton-proton and proton-nucleus collisions. The antinuclei production in ion-ion collisions will be quoted only for completeness.

– As mentioned in the introduction, the experimental data on the production of mass-3 antinuclei are extremely scarce, and much less informative than that on antideuteron production, with only two experiments or sets of experiments reporting on mass-3 antinuclei production in proton-nucleus collisions [8–11]. Note that there are no experimental data available on the production of these antinuclei in proton-proton collisions. The production of $\overline{^3\mathrm{He}}$ has been observed recently in various heavy-ion studies like Pb + Pb collisions at ultra-relativistic incident energies [16]. These data are out of the scope of the present work. They will not be discussed here (see [3] for a discussion).
– Coalescence calculations require the antiproton production cross-section to be known for antiproton momenta equal to approximately one third of the $A = 3$ antinuclei momenta. Unfortunately, in most experiments the differential cross-sections for antiproton and $A = 3$ antinuclei productions were not measured at this momentum. The $\overline{p}$ cross-section thus had to be extrapolated to the appropriate kinematical region when no other data were available, which of course, introduces additional uncertainty in the calculations.

The three-nucleon wave functions needed in the calculations are much less well know than the deuteron wave function. In addition, the same wave function will be used for ^{3}He and t nuclei (see appendix A). The inaccuracy on the trinucleon wave functions is thus another source of uncertainty. Nevertheless, the same 3-nucleon wave function used in the present work has been used previously to successfully account for the ^{3}He spectrum in [6]. So this source of uncertainty in not the most important.

The total reaction cross-section used in the calculations was described by means of the parameterization proposed in [17].

4.2 Proton-aluminium collision data at 70 GeV/c

The antinuclei produced in the Serpukhov experiments [8, 9] were obtained from a 70 GeV/c proton beam incident on an aluminium target at 27 mrad scattering angles and 20 GeV/c for $\overline{^3\mathrm{He}}$, and 0° and 25 GeV/c for $\overline{t}$. The inclusive antiproton cross-sections were available from [18] and [19] in the same kinematical conditions.

In fig. 4 the $\overline{p}$ cross-section data from [8] are compared with the results of fits using a functional form [20] (the simple Gaussian form in (4) is no more used for the $\overline{p}$ inclusive cross-section, see sect. 3). The solid curve corresponds to a fit of a large sample of $p + A \to \overline{p}$ data (654 experimental points) from 12 up to 400 GeV incident energies not including those from ref. [8] which were found not to be compatible with the other sets of data [20] (see appendix B). The calculated values are in fair agreement with the two lowest-momentum data points (which were obtained by extrapolation from measurements at other angles). They overestimate the other data points by a factor of 2 to 4. The dotted curve is a renormalization of the solid curve by a factor ≈ 2.5 to fit these latter points, while the dashed curve corresponds to the fit of the single set of data points shown in the figure, whose parameters, however, give quite poor agreement with the other sets of data [20].

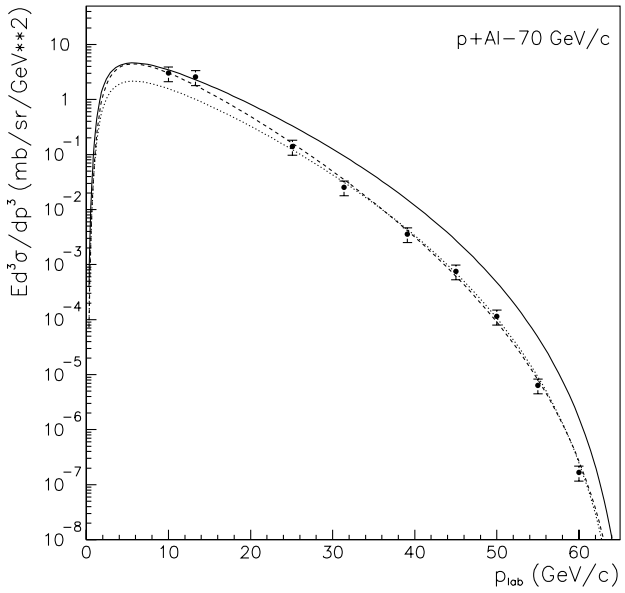

Fig. 4. Inclusive differential cross-section for antiproton production in $p + \mathrm{Al}$ collisions as a function of the total momentum in the laboratory frame from [8], compared to calculated values as discussed in the text. p_{lab} is the total momentum. The measures are made at zero degree scattering angles in the laboratory frame and the two first points were obtained by extrapolation from measurements at other angles.

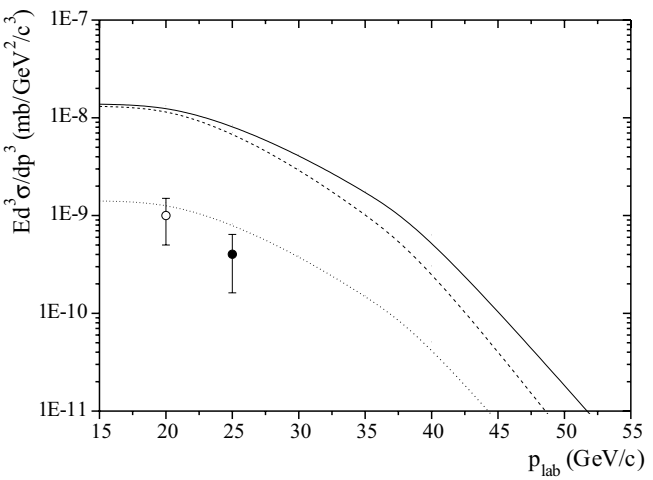

Fig. 5. The inclusive differential cross-section for $\overline{t}$ [8] (open circles) and $\overline{^3\mathrm{He}}$ [9] (black circles) production by 70 GeV protons on Al target compared to calculations using the microscopic model of coalescence and the same three different parameterizations of the antiproton production cross-section as shown in fig. 4, with the same graphical conventions. p_{lab} is the total momentum. The measures are made at 27 mrad scattering angles for $\overline{^3\mathrm{He}}$ and 0 for $\overline{t}$ in the laboratory frame.

It must be emphasized that the low-momentum region, say $p_{\mathrm{lab}} < 10$ GeV/c, which is the useful region for the coalescence calculations, with $\mathbf{p}_{\overline{p}} \approx \mathbf{p}_{\overline{t}}/3$ is particularly important here, with unfortunately no data point from direct measurement available over the relevant range.

Figure 5 compares the calculations for the $A = 3$ production cross-section for the three parameterizations shown in fig. 4 with the experimental data. The calculations using the global fit renormalized to the 70 GeV/c data (see fig. 4) give by far the best agreement with the $\overline{t}$ data (dotted curve). The other two sets of $\overline{p}$ cross-section parameters overestimate the data by a sound order of magnitude. This is apparently consistent with the larger $\overline{p}$ cross-section predicted by these two sets of parameters for the low-$\overline{p}$ momentum region to which the $\overline{t}$ cross-section is most sensitive. The factor of about 2 between the $\overline{p}$ cross-sections predicted by the two groups of parameters translates into a factor of about 10 for the $\overline{t}$ cross-section because of the approximately cubic dependence of the latter on the $\overline{p}$ cross-section. However, it is somewhat puzzling that this agreement is obtained with parameters which are not consistent with the whole body of $\overline{p}$ data [20].

4.3 Proton-beryllium collision data at 200 GeV/c

In the CERN experiments [10,11], $\overline{p}$, $\overline{t}$ and $\overline{^3\mathrm{He}}$ were produced in proton-beryllium collisions at 200, 210, and 240 GeV/c and detected at 0 degree scattering angle [11], while $\overline{p}$ were measured at 200 GeV/c [10] on the same targets. For these data, however, the production cross-sections were measured as the ratios to the π^- production cross-sections at the same momentum. The knowledge of the corresponding experimental π^- production cross-section, or a good parameterization of the latter, is thus required in order to allow the values of the $\overline{p}$, $\overline{t}$ and $\overline{^3\mathrm{He}}$ production cross-sections to be calculated.

Table 1. Values of the parameters of relation (16) obtained by fitting the π^- production cross-sections for 200 and 300 GeV/c protons on beryllium.

Parameter	C_1	C_2	C_3	C_4
Value	0.94	1.88	7.05	1.69

Fortunately, the $p + \mathrm{Be} \rightarrow \pi^- + X$ cross-section has been measured at 200 and 300 GeV/c incident momentum in [21] in similar kinematical conditions as in the CERN experiment. The measured distributions have been fit by means of the following functional form, inspired from ref. [22]:

$$E\frac{\mathrm{d}^3\sigma}{\mathrm{d}p^3}\left(\pi^-\right) = C_1\sigma_{\mathrm{in}}\left(1-x\right)^{C_2} e^{-C_3 x} e^{-C_4 p_\perp}\,, \qquad (16)$$

where $x = E^*/E^*_{\mathrm{max}}$ (E^* is the total energy of the inclusive particle in the center-of-mass frame, σ_{in} is the total reaction cross-section for the system in collision, $\sqrt{s}$ is the total energy of the system and $p_\perp$ the transverse momentum of the emitted particle). The values of the parameters obtained are given in table 1 and the results of this fit are presented in fig. 6. The parameterization (16) has been used to extract the experimental $\overline{p}$ production cross-sections [10]. The resulting cross-section values are compared in fig. 7 with the results of the fit of a functional form

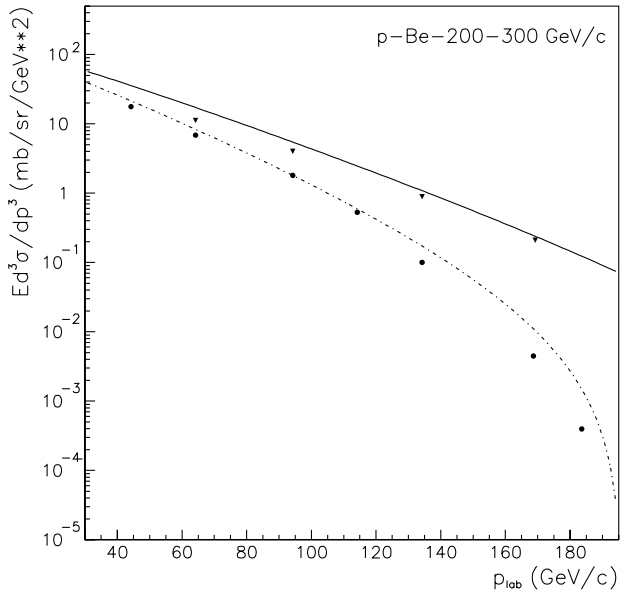

Fig. 6. Experimental inclusive differential cross-section for π^- production in $p + \mathrm{Be}$ collisions [21] at 200 GeV/c (full circles) and 300 GeV/c (full triangles) compared with the functional form (16). p_{lab} is the total momentum. The measures are made at 3.6 mrad scattering angles in the laboratory frame.

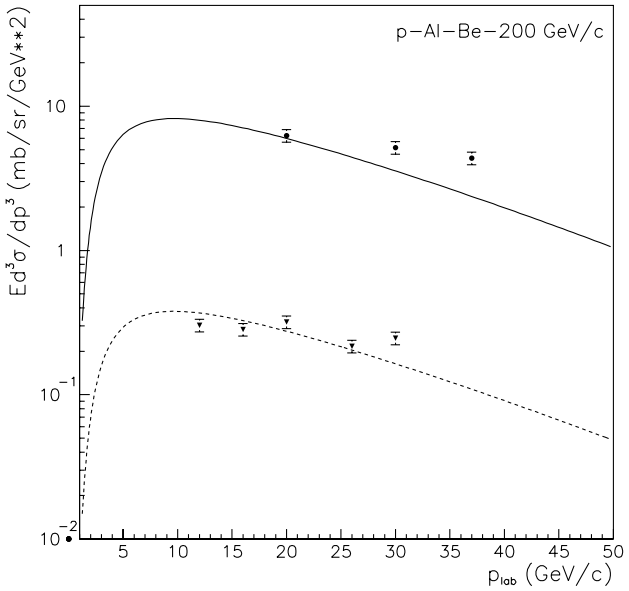

Fig. 7. Experimental inclusive differential cross-sections for $\overline{p}$ production in $p + \mathrm{Al}$ collision (circles), and in $p + \mathrm{Be}$ collision ($\times 10^{-1}$, triangles), [18] compared with the results of fits using a functional form (curves) [20]. p_{lab} is the total momentum. The measures are made at 0 mrad scattering angles in the laboratory frame.

to a large sample of $p+A \to \overline{p}+X$ data from 12 GeV/c up to 400 GeV/c incident momenta [20]. It is seen that the data points derived previously and the calculated values are in fair agreement. This consistency gives confidence to the following steps of the analysis for the evaluation of the $\overline{t}$ and $\overline{^3\mathrm{He}}$ production cross-sections. In fig. 8, the $\overline{t}$ and $\overline{^3\mathrm{He}}$ production cross-sectionsare compared to

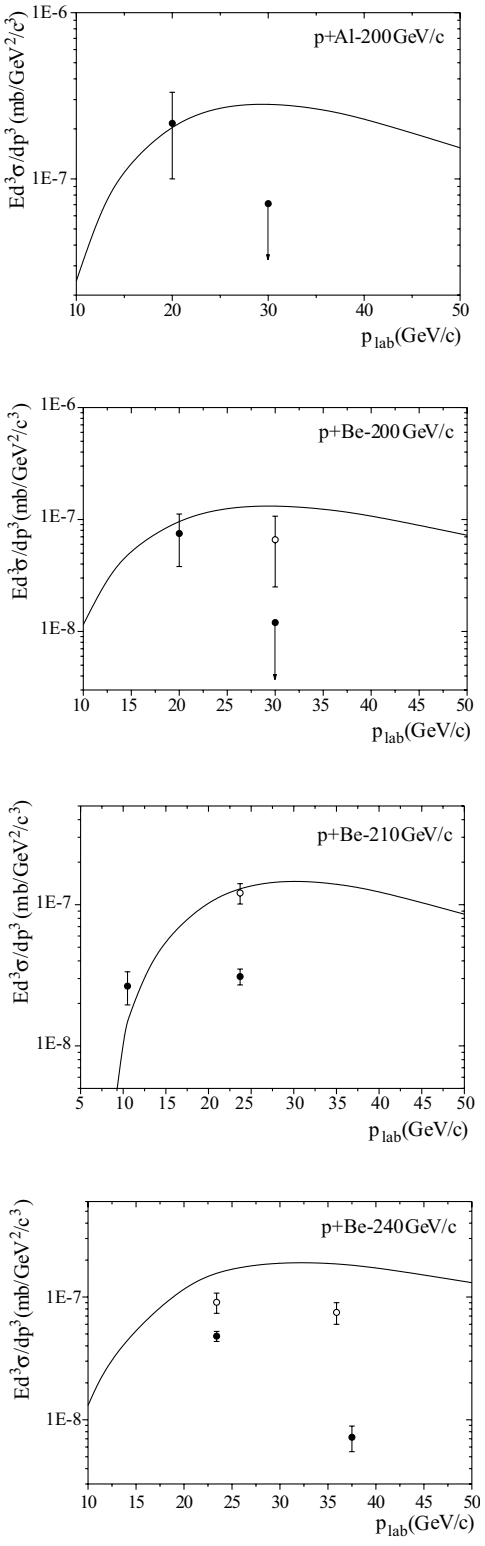

Fig. 8. Experimental inclusive differential cross-section for $\overline{t}$ (full circles) and $\overline{^3\mathrm{He}}$ (open circles) production in $p + \mathrm{Al}$ and $p + \mathrm{Be}$ collisions, compared to calculations using the microscopic model of coalescence (solid line). p_{lab} is the total momentum. The measures are made at 0 mrad scattering angles in the laboratory frame.

calculations using the microscopic model of coalescence. The agreement between experimental and calculated values varies from poor to good. On the average, however, data and calculations are within one order of magnitude. This result should be considered as a success in account of the numerous sources of uncertainties of the calculations and of the limited accuracy of the measurements. Note also that refs. [10] and [11] report experimental values in disagreement by a factor of 2. Furthermore the $\overline{t}$ and $\overline{^3\mathrm{He}}$ production cross-sections, measured at the same momentum, should be in principle close to each other (this fact is clearly seen in the same experiment for t and ^{3}He production), whereas, in this experiment, they are quite different.

In terms of the usual coalescence model [4], the results shown in fig. 8 correspond to a coalescence momentum in the range 150–200 MeV. This is compatible with the accepted value of the coalescence momentum for light nuclei formation [4]. For the Serpukhov data, the dotted curve in fig. 4 corresponds to a coalescence momentum in the range 270–280 MeV, which is much higher. These latter data, however, were found inconsistent with the other available data in some respects in [20].

5 Conclusion

It has been shown in this work that the diagrammatic approach to the coalescence model developed previously can successfully (within the experimental uncertainties) account for the mass-3 antinuclei production cross-section in proton-nucleus collisions over wide kinematical conditions without any additional parameter. These calculations require a good knowledge of the antiproton production cross-section. These results would be further used to calculate $\overline{t}$ and $\overline{^3\mathrm{He}}$ flux in cosmic rays.

Appendix A.

In this appendix, we briefly remind how the wave functions of the trinucleon is written in [14], while in this paper slightly different definitions have been used. A useful analytical parameterization of the bound trinucleon wave function is obtained from solving the Faddeev equation with the Reid soft-core potential.

The total wave function of the triton is written as a sum of 3 Faddeev components:

$$\Psi = \sum_{i=1}^{3} \Psi_t^i \left(\mathbf{q}_i, \mathbf{p}_i\right) .$$

In (9)-(13), we make use of only one Faddeev component Ψ_t, while, due the exchange symmetry of two-nucleons in the triton, all the three Faddeev components are identical. Furthermore, Faddeev components Ψ_t are decomposed in terms of their partial-wave components with respect to the spin-isospin and angular-momentum basis $\phi_\alpha(\hat{\mathbf{p}}, \hat{\mathbf{q}})$:

$$\Psi_t(\mathbf{p}, \mathbf{q}) = \sum_\alpha \psi_\alpha(p, q)\phi_\alpha(\hat{\mathbf{p}}, \hat{\mathbf{q}}) ,$$

with, if $\mathbf{p}_i$ $(i = 1, 2, 3)$ is the nucleon momentum

$$\mathbf{p} = \frac{1}{2}\left(\mathbf{p}_1 - \mathbf{p}_2\right), \mathbf{q} = \frac{1}{2\sqrt{3}}\left(\mathbf{p}_1 + \mathbf{p}_2 - 2\mathbf{p}_3\right) .$$

The following normalization is used

$$\int \left|\Psi_t\left(\mathbf{p}, \mathbf{q}\right)\right|^2 \mathrm{d}^3\mathbf{p}\mathrm{d}^3\mathbf{q} = \sum_\alpha \int \mathrm{d}p\mathrm{d}q p^2 q^2 \left|\psi_\alpha\left(p, q\right)\right|^2 = 1 .$$

Note that, in these expressions, the definition of $\mathbf{p}$ and the normalization differ from (6) and (10). Ψ_t is a sum of the partial-wave states α which is a label for the following physical quantities:

- L, the angular momentum of the pair of nucleons (1-2),
- l, the angular momentum of nucleon 3 according to the center of the mass of the pair of nucleons (1-2),
- $\mathcal{L}$, the total angular momentum of the triton.
- s, the spin of the pair of nucleons (1-2),
- $\mathcal{S}$, the total spin of the triton,
- T, the isospin of the pair of nucleons (1-2).

Only two components with label α were taken into account, $\alpha = 1, 2$.

- For $\alpha = 1$, $L = l = \mathcal{L} = 0$, $s = 1$, $\mathcal{S} = 1/2$ and $T = 0$.
- For $\alpha = 2$, $L = l = \mathcal{L} = s = 0$, $\mathcal{S} = 1/2$ and $T = 1$.

Of course, the fact to consider only two partial-wave states is an approximation which gives the probability of 89.25% of trinucleon being in the partial-wave state α. In [14], the parameterization for $\psi_\alpha\left(p, q\right)$ is given by

$$\psi_\alpha\left(p, q\right) = p^L p^l \left(p^2 + \Omega_{p1}^2\right)^{-1} \prod_{m=1}^{3} \left(q^2 + \Omega_{qm}^2\right)^{-1} \times \sum_{i=1}^{6}\sum_{j=1}^{6} \frac{C_{ij}}{\left(p^2 + \mu_i^2\right)\left(q^2 + \nu_j^2\right)},$$

with Ω_{p1}, Ω_{qm}, μ_i, ν_j and C_{ij} all depending on the partial-wave label α. The numerical values of these coefficients can be found in [14].

^{3}He(ppn) and $t(pnn)$ are considered to have the same wave function. Altough, because of the presence of the Coulomb interaction, these two wave functions are slightly different, this difference is negligible compared to the other uncertainties of present calculations.

Appendix B.

For the reader's convenience, the parameterization of the antiproton inclusive production from [20] and used in sect. 4 is briefly described. A large number of $p+A \to \overline{p}+X$ experimental data from 12 GeV/c up to 400 GeV/c and $1 \leq A \leq 208$ have been used. The agreement obtained with the data is good.

The following functional form has been proposed:

$$E\frac{\mathrm{d}^3\sigma}{\mathrm{d}p^3} = \sigma_{\mathrm{ine}} A^{C_1 \ln\left(\frac{\sqrt{s}}{C_2}\right) p_\perp} \left(1 - x_{\mathrm{R}}\right)^{C_3 \ln\left(\sqrt{s}\right)} e^{-C_4 x_{\mathrm{R}}} \times \left[\left(\sqrt{s}\right)^{C_5} C_6 e^{-C_7 p_\perp} + \left(\sqrt{s}\right)^{C_8} C_9 e^{-C_{10} p_\perp^2}\right] ,$$

Table 2. Values of the parameters C_1 from C_{10}.

Parameter	C_1	C_2	C_3	C_4	C_5
Value(error)	0.16990(4)	10.28(13)	2.269(7)	3.707(27)	0.009205(2)
Parameter(error)	C_6	C_7	C_8	C_9	C_{10}
Value	0.4812(14)	3.3600(2)	0.063940(15)	−0.1824(15)	2.4850(6)

where A is the mass target, $x_{\mathrm{R}} = E^*/E^*_{\mathrm{max}}$ the radial scaling variable. E^* and E^*_{max} are the total energy of the inclusive particle and its maximum possible energy in the center-of-mass frame, respectively. $p_\perp$ is the component of momentum transverse to the beam direction. $\sqrt{s}$ is the total centre-of-mass energy and σ_{ine} is the total inelastic cross-section. The parameters C_1 from C_{10} are given in table 2.

References

1. See sect. IV in Nucl. Phys. B Proc. Suppl. **113** (2002).
2. O. Adrani *et al.*, Nucl. Instrum. Methods A **478**, 114 (2002).
3. R.P. Duperray, K.V. Protasov, A.Yu. Voronin, Eur. Phys. J. A **16**, 27 (2003).
4. S.T. Butler, C.A. Pearson, Phys. Rev. Lett. **7**, 69 (1961); Phys. Lett. **1**, 77 (1962); Phys. Rev. **129**, 836 (1963); A. Schwarzschild, C. Zupancic, Phys. Rev. **129**, 854 (1963); L.P. Csernai, J.I. Kapusta, Phys. Rep. **131**, 223 (1985).
5. See, for example, the classical paper by S. Nagamyia *et al.*, Phys. Rev. C **24**, 971 (1981) and Nucl. Phys. A **661** (1999) for recent references.
6. V.M. Kolybasov, Yu.N. Sokol'skikh, Phys. Lett. B **225**, 31 (1989); Sov. J. Nucl. Phys. **55**, 1148 (1992).
7. P. Chardonnet, J. Orloff, P. Salati, Phys. Lett. B **409**, 313 (1997).
8. Y.M. Antipov *et al.*, Phys. Lett. B **34**, 164 (1971).
9. N.K. Vishnevskii *et al.*, Sov. J. Nucl. Phys. **20**, 371 (1974).
10. W. Bozzoli *et al.*, Nucl. Phys. B **144**, 317 (1978).
11. A. Bussière *et al.*, Nucl. Phys. B **174**, 1 (1980).
12. M.A. Braun, V.V. Vechernin, Sov. J. Nucl. Phys. **44**, 506 (1986); **36**, 357 (1982).
13. I.S. Shapiro, *Dispersion theory of direct nuclear reactions*, in *Selected Topics in Nuclear Theory*, edited by F. Janouch (IAEA, Vienna, 1963); Usp. Fiz. Nauk **92**, 549 (1967) (Sov. Phys. Usp. **10**, 515 (1968)).
14. Muslim, Y.E. Kim, Nucl. Phys. A **427**, 235 (1984).
15. F. James, Monte Carlo Phase Space, CERN 68-15 (1968); `http://wwwinfo.cern.ch/asdoc/shortwrupsdir/w515/top.html`.
16. G. Appelquist *et al.*, Phys. Lett. B **376**, 245 (1996); see Nucl. Phys A **661** (1999) for more on this issue.
17. J.R. Letaw, R. Silberberg, C.H. Tsao, Astrophys. J. Suppl. Ser. **51**, 271 (1983).
18. F. Binon *et al.*, Phys. Lett. B **30**, 510 (1969).
19. Yu.B. Bushnin *et al.*, Sov. J. Nucl. Phys. **10**, 337 (1970).
20. R.P. Duperray, C.Y. Huang, K.V. Protasov, M. Buénerd, to be published in Phys. Rev. D **68** (2003), astro-ph/0305274.
21. W.F. Baker *et al.*, Phys. Lett. B **51**, 303 (1974).
22. A.N. Kalinovskii, N.V. Mokhov, Yu.P. Nikitin, *Passage of High-Energy Particles Through Matter* (American Institute of Physics, New York, 1989).